J|A|C|S
ARTICLES
Published on Web 11/17/2006

Toward Monodispersed Silver Nanoparticles with Unusual Thermal Stability

Junming Sun,[†] Ding Ma,[†] He Zhang,[†] Xiumei Liu,[†] Xiuwen Han,[†] Xinhe Bao,*[,†] Gisela Weinberg,[‡] Norbert Pfänder,[‡] and Dangsheng Su[‡]

Contribution from the State Key Laboratory of Catalysis, Dalian Institute of Chemical Physics, Chinese Academy of Sciences, Dalian 116023, People's Republic of China, and Department of Inorganic Chemistry, Fritz-Haber Institute of the Max Planck Society, Berlin D-14195, Germany

Received July 10, 2006; E-mail: xhbao@dicp.ac.cn

Abstract: A novel *in situ* autoreduction route has been developed, by which monodispersed silver nanoparticles with tunable sizes could be easily fabricated on silica-based materials, especially inside the channels of mesoporous silica (MPS). ^{13}C CP/MAS NMR spectroscopy was employed to monitor the whole assembly process. It was demonstrated that the amino groups of APTS (aminopropyltriethoxyl silane)-modified MPS can be used to anchor formaldehyde to form novel reducing species ($NHCH_2OH$), on which $Ag(NH_3)_2NO_3$ could be *in situ* reduced. Monodispersed silver nanoparticles were thus obtained. *In situ* XRD and *in situ* TEM experiments were used to investigate and compare the thermal stabilities of silver nanoparticles on the external surface of silica gels (unconfined) and those located inside the channels of SBA-15 (confined). It was observed that unconfined silver nanoparticles tended to agglomerate at low temperatures (i.e., lower than 773 K). The aggregation of silver nanoparticles became more serious at 773 K. However, for those confined silver nanoparticles, no coarsening process was observed at 773 K, much higher than its Tammann temperature (i.e., 617 K). Only when the treating temperature was higher than 873 K could the agglomeration of those confined silver nanoparticles happen with time-varying via the Ostwald ripening process. The confinement of mesopores played a key role in improving the thermal stabilities of silver nanoparticles (stable up to 773 K without any observable coarsening), which is essential to the further investigations on their chemical (e.g., catalytic) properties.

1. Introduction

Ultra fine metal (or metal nanoparticles) catalysts are widely used in industry as well as in laboratory.[1−3] With the development of catalysis science, increasing attention has been paid to the size-dependent chemistry of nanocatalysis,[4−5] which elucidates the correlations between the activity and particle size.[6] As an example, gold nanoparticles show amazingly high activity toward low-temperature oxidation of carbon monoxide.[7] Quantum size effect that emerged from the reduction of gold particle size, especially when the diameter is less than 3 nm, is responsible for the high activity. However, it must be kept in mind that most of the catalytic reactions are high-temperature processes, where bare metal nanoparticles (those without the protection of protective agents) tend to agglomerate.[8] At the same time, sintering of metal is strongly temperature-dependent and closely related to the so-called Tammann temperature ($T_{Tammann} = 0.5T_F$; T_F represents the melting point). When the Tammann temperature is reached, bulk atoms tend to move, which leads to interparticle diffusion and therefore coalescence of metal particles. It is reported that when the particle size comes into nanorange, the melting point of those metal nanoparticles decreased drastically with the decrease of the particle size, resulting in a much lower thermal stability.[9] The low thermal stability of metal nanoparticles limits their applications inevitably. Traditionally, inert inorganic matrix hosts (e.g., SiO_2, Al_2O_3, etc.) were often used to suppress the sintering of the metal nanoparticles. Unfortunately, as most of those hosts are mainly structurally nonuniform, the size and shape of the obtained metal nanoparticles were difficult to be controlled and thus in most cases randomly distributed. As a result, the catalytic properties of these supported nanocatalysts are not well understood.[3]

Recently, the discovery of mesoporous silicas, such as M41s[10] and SBA-15,[11] has initiated intensive research of inclusion chemistry inside the channels of mesoporous silicas.[12−14] Due to their uniform mesostructures, high surface areas, and tunable

[†] Chinese Academy of Sciences.
[‡] Fritz-Haber Institute of the Max Planck Society.

(1) Bell, A. T. *Science* **2003**, *299*, 1688.
(2) Hughes, M. D.; Xu, Y. J.; Jenkins, P.; McMorn, P.; Landon, P.; Enache, D. I.; Carley, A. F.; Attard, G. A.; Hutchings, G. J.; King, F.; Stitt, E. H.; Johnston, P.; Griffin, K.; Kiely, C. J. *Nature* **2005**, *437*, 1132. Schlögl, R.; Hamid, S. B. A. *Angew. Chem., Int. Ed.* **2004**, *43*, 1628.
(3) Gates, B. C. *Chem. Rev.* **1995**, *95*, 511.
(4) Rao, C. N. R.; Kulkarni, G. U.; Thomas, P. J.; Edwards, P. P. *Chem. Eur. J.* **2002**, *8*, 28 and references therein.
(5) Bukhtiyarov, V. I.; Slin'ko, M. G. *Russ. Chem. Rev.* **2001**, *70*, 147 and references therein.
(6) Schalow, T.; Brandt, B.; Starr, D. E.; Laurin, M.; Shaikhutdinov, S. K.; Schauermann, S.; Libuda, J.; Freund, H.-J. *Angew. Chem., Int. Ed.* **2006**, *45*, 3693.
(7) Haruta, M.; Tsubota, S.; Kobayashi, T.; Kageyama, H.; Genet, M. J.; Delmon, B. *J. Catal.* **1993**, *144*, 175. Goodman, D. W. *J. Catal.* **2003**, *216*, 213.
(8) Kizuka, T.; Ichinose, H.; Ishida, Y. *J. Mater. Sci.* **1997**, *32*, 1501.
(9) Buffat, Ph.; Borel, J. -P. *Phys. Rev. A* **1976**, *13*, 2287.

10.1021/ja064884j CCC: $33.50

pore sizes,[11,15] these ordered mesoporous silicas have been found to be the promising templates to control the shape and size of the occluded metal nanoparticles,[16−32] which have potential applications in catalysis.[33] Current methodologies for the assembly of metal nanoparticles inside the channels of mesoporous silica include conventional incipient wetness impregnation,[16−17] metal−organic chemical vapor deposition (MOCVD),[18] and schemes making use of the silanols on the internal channels,[23−27] etc. Metals such as Au, Pd, Pt, etc., have been successfully encapsulated inside the channels of mesoporous materials.[23,25−26,28−30]

As a relatively inexpensive metal, silver has been extensively studied in the field of catalysis (e.g., selective oxidation of methanol, oxidative coupling of methane, and ethylene epoxidation, etc.).[34−36] However, due to the low melting point (ca. 1233 K) and thus the low T_{Tammann} (ca. 617 K) of silver, sintering of silver nanoparticles during the high-temperature reactions (e.g., methanol oxidation) becomes one of the scientifically most important and challenging problems. To use a nanocatalyst in high-temperature reactions, one solution is to confine the nanoparticles within a host (i.e., mesoporous materials) that could prevent those particles from sintering. However, due to the strong diffusion ability of ionic metals (in this case, Ag^+) via hydroxyl groups,[29] encapsulation is much more difficult inside mesoporous channels, especially in terms of particle homogeneity. Although many efforts have been made,[24,27,29,31] metal nanowires or a mixture of nanowires and nanoparticles were often the result because of the limitation of the mesostructures themselves or the lack of an effective control over the synthesis.[28,31] Herein, we present a general route by which nearly monodispersed silver nanoparticles could be fabricated on the surface (internal or external) of silica-based materials, and noteworthy, monodispersed silver nanoparticles can be selectively assembled inside the channels of mesoporous silicas. ^{13}C CP/MAS NMR spectroscopy was employed to monitor the whole assembly process. It was observed that the amino groups of APTS (aminopropyltriethoxyl silane)-modified MPS can be used to anchor formaldehyde to form $NHCH_2OH$ species, on which $Ag(NH_3)_2NO_3$ could be *in situ* reduced. *In situ* XRD and *in situ* TEM experiments were used to compare the thermal stabilities of unconfined and confined silver nanoparticles. It was observed that silver nanoparticles located inside the mesopores showed unusual thermal stabilities (stable up to 773 K, which is far higher than its Tammann temperature (i.e., 617 K)). The confinement of ordered mesopores played a crucial role in improving the thermal stabilities of silver nanoparticles, which is essential to the further investigations on their chemical (e.g., catalytic) properties.[34−36]

2. Experimental Section

2.1. Materials Synthesis. Mesoporous silicas (MPS, such as SBA-15) were synthesized according to the published procedure.[11,15,37] An amount of 2.0 g as-synthesized MPS (herein, MPS represents SBA-15, MCM-41, and FDU-12) was suspended in 150 mL pure toluene under flowing N_2, and then 10 mL TMCS (trimethylchlorosilane) was added dropwise under stirring. The mixture was recovered by filtration with toluene and ethanol after stirring continuously at 353 K for 8 h. After that, templates (e.g., P123) that occluded inside the samples can be removed by solvent extraction or by calcination at 623−673 K for 6 h. Here, the calcinations method was used. Thus, the mesoporous silicas with the external surface functionalized with $Si(CH_3)_3$ (assigned as TMCS-MPS) were obtained. An amount of 2.0 g TMCS-MPS was dried at 373 K for 12 h before dispersion in 150 mL toluene. Then 6.0 mL APTS (aminopropyltriethoxyl silane) was added under stirring. The mixture obtained was stirred for another 12 h at room temperature and refluxed at 353 K for 8 h. The recovered solid was washed with toluene and then with ethanol intensively to remove the physically adsorbed APTS and toluene. The selectively functionalized sample was denoted as APTS-TMCS-MPS (if SBA-15 was used, then the sample was denoted as APTS-TMCS-SBA-15), after being vacuum-dried at 353 K for more than 6 h. Reducing species were introduced by stirring 1.0 g APTS-TMCS-MPS in a 105 mL mixture of formaldehyde, ethanol and water (formaldehyde/ethanol/water = 5:20:80, v/v/v) at 313 K for 30 min. The filtered solid was dried at 323 K for 12 h and named as HCHO-APTS-TMCS-MPS. To introduce Ag, 1.0 g HCHO-APTS-TMCS-MPS was added into a mixture of ethanol and $Ag(NH_3)_2NO_3$-(aq) (ethanol/$Ag(NH_3)_2NO_3$(aq) = 1:4, v/v). $Ag(NH_3)_2NO_3$(aq) solution (0.005 M) was prepared by dropwise addition of NH_3(aq) into $AgNO_3$ aqueous solution until the formation of a clear colorless solution. The HCHO-APTS-TMCS-MPS/$Ag(NH_3)_2NO_3$ mixture was then stirred at 313 K for 30 min before filtration. The filtered yellowish or brown product was rinsed with large amounts of deionized water and dried at 323 K for 12 h to get Ag-1/MPS (in the case of SBA-15, Ag-1/SBA-15). In the control experiments, the same procedure was followed except for the HCHO treatment. The sample complexed with silver ions was calcined at 573 K to get the metallic Ag inside channels, which was

(10) Kresge, C. T.; leonowicz, M. E.; Roth, W. J.; Vartuli, J. C.; Beck, J. S. *Nature* **1992**, *359*, 710.
(11) Zhao, D.; Feng, J.; Huo, Q.; Melosh, N.; Fredrickson, G. H.; Chmelka, B. F.; Stucky, G. D. *Science* **1998**, *279*, 548.
(12) Corma, A. *Chem. Rev.* **1997**, *97*, 2373 and references therein.
(13) Moller, K.; Bein, T. *Chem. Mater.* **1998**, *10*, 2950 and references therein.
(14) Shi, J. L.; Hua, Z. L.; Zhang, L. X. *J. Mater. Chem.* **2004**, *14*, 795 and references therein.
(15) Zhang, H.; Sun, J. M.; Ma, D.; Bao, X. H.; Klein-Hoffmann, A.; Weinberg, G.; Su, D. S.; Schlögl, R. *J. Am. Chem. Soc.* **2004**, *126*, 7440. Sun, J. M.; Zhang, H.; Ma, D.; Chen, Y.; Bao, X. H.; Klein-Hoffmann, A.; Pfänder, N.; Su, D. S. *Chem. Commun.* **2005**, 5343.
(16) Junges, U.; Jacobs, W.; Voigt-Martin, I.; Drutzsch, B.; Schüth, F. *Chem. Commun.* **1995**, 2283.
(17) Fishel, C. T.; Davis, R. J.; Garces, J. M. *J. Catal.* **1996**, *163*, 148.
(18) Lee, K. B.; Lee, S. M.; Cheon, J. *Adv. Mater.* **2001**, *13*, 517.
(19) Corma, A.; Martinez, A.; Martinez-Soria, V. J. *J. Catal.* **1997**, *169*, 480.
(20) Ryoo, R.; Ko, C. H.; Kim, J. M.; Howe, R. *Catal. Lett.* **1996**, *37*, 29.
(21) Han, Y. J.; Kim, J. M.; Stucky, G. D. *Chem. Mater.* **2000**, *12*, 2068.
(22) Liu, Z.; Sakamoto, Y.; Ohsuna, T.; Hiraga, K.; Terasaki, O.; Ko, C. H.; Shin, H.-J.; Ryoo, R. *Angew. Chem., Int. Ed.* **2000**, *39*, 3107.
(23) Guari, Y.; Thieuleux, C.; Mehdi, A.; Reyé, C.; Corriu, R. J. P.; Gomez-Gallardo, S.; Philippot, K.; Chaudret, B.; Dutartre, R. *Chem. Commun.* **2001**, 1374.
(24) Zhang, W. H.; Shi, J. L.; Wang, L. Z.; Yan, D. S. *Chem. Mater.* **2000**, *12*, 1408. Tu C. H.; Wang, A. Q.; Zheng, M. Y.; Meng, Y.; Shan, J. H.; Zhang, T. *Chin. J. Catal.* **2005**, *26*, 631.
(25) Yang, C. M.; Liu, P. H.; Ho, Y.; Chiu, C.; Chao, K. *Chem. Mater.* **2003**, *15*, 275.
(26) Li, L.; Shi, J. L.; Zhang, L. X.; Xiong, L. M.; Yan, J. N. *Adv. Mater.* **2004**, *16*, 1079.
(27) Zhao, X. G.; Shi, J. L.; Hu, B.; Zhang, L. X.; Hua, Z. L. *Mater. Lett.* **2004**, *58*, 2152.
(28) Fukuoka, A.; Araki, H.; Kimura, J.; Sakamoto, Y.; Higuchi, T.; Sugimoto, N.; Inagaki, S.; Ichikawa, M. *J. Mater. Chem.* **2004**, *14*, 752.
(29) Besson, S.; Gacoin, T.; Ricolleau, C.; Boilot, J. P. *Chem. Commun.* **2003**, 360.
(30) Zhu, J.; Kónya, Z.; Puntes, V. F.; Kiricsi, I.; Miao, C. X.; Ager, J. W.; Alivisatos, A. P.; Somorjai, G. A. *Langmuir* **2003**, *19*, 4309.
(31) Huang, M. H.; Choudrey, A.; Yang, P. D. *Chem. Commun.* **2000**, 1063.
(32) Bao, X. H.; Sun, J. M; Zhang, H. C. N. Patent CN1698954, 2005. Chen, Y.; Wang, C. A.; Liu, H. Y.; Qiu, J. S.; Bao, X. H. *Chem. Commun.* **2005**, *42*, 5298.
(33) Taguchi, A.; Schüth, F. *Micropor. Mesopor. Mater.* **2005**, *77*, 1. Sayari, A. *Chem. Mater.* **1996**, *8*, 1840.
(34) Bao, X.; Muhler, M.; Schlogl, R.; Ertl, G. *Catal. Lett.* **1995**, *32*, 185. van Veen, A. C.; Hinrichsen, O.; Muhler, M. *J. Catal.* **2002**, *210*, 53.
(35) van Santen, R. A.; Kuipers, H. P. C. *Adv. Catal.* **1987**, *35*, 265 and references therein.
(36) Qu, Z. P.; Cheng, M. J.; Huang, W. X.; Bao, X. H. *J. Catal.* **2005**, *229*, 446.
(37) Fan, J.; Yu, C. Z.; Lei, J.; Zhang, Q.; Li, T. C.; Tu, B.; Zhou, W. Z.; Zhao, D. Y. *J. Am. Chem. Soc.* **2005**, *127*, 10794.

Scheme 1. Schematic Representation of Assemblage of Highly Dispersed Ag Nanoparticles Inside the Channels of SBA-15

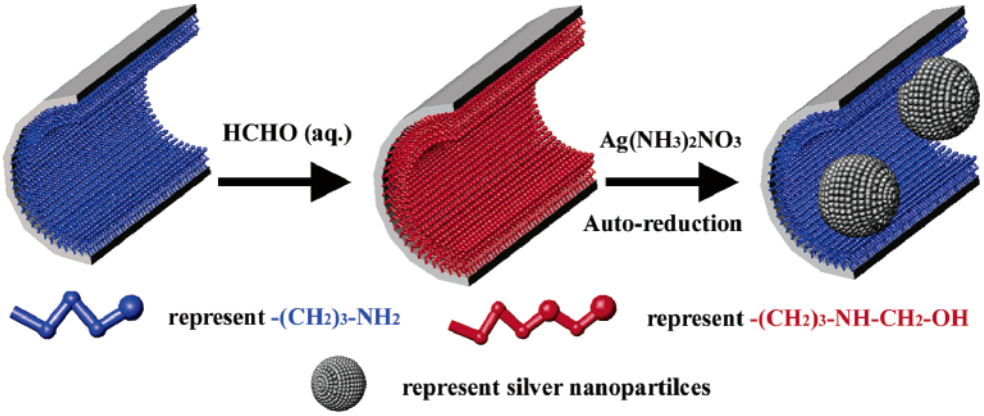

denoted as Ag-2/MPS. A sample without TMCS treatment but following the same procedure to Ag-1/MPS, was also prepared and denoted as Ag-3/MPS.

In the control experiments, silica gel (SiO_2) was bought from Qingdao Ocean Chemical Ltd. Surface areas is ca. 238 m^2/g, and average pore size is more than 20 nm (Figure S1). Preparation of Ag/SiO_2 follows that of Ag-3/MPS. It should be mentioned that the porosity and surface area of the silica gel are created by the aggregated primary nonporous silica particles.[38] Therefore, the obtained monodispersed silver nanoparticles are actually located on the external surface of SiO_2 spheres (in the current case, the diameters of the primary silica particles are smaller than 50 nm). Thus, those silver nanoparticles are called unconfined silver nanoparticles

2.2. Characterization. NMR spectra were recorded on a Varian infinity-plus 400WB solid-state NMR spectrometer. SEM images were taken on the Hitachi S4000 and S4800 scanning electron microscopes. All samples were observed directly without coating any metal or carbon. In addition, to get clearer contrast of silver nanoparticles, 15−70% BSE signals are introduced in the secondary electrons. The TEM images were obtained with a Philips CM 200 Transmission Electron Microscope equipped with a CCD camera. The samples were embedded in epoxy resin and cut into slices for TEM characterization.

X-ray diffraction (XRD) patterns were collected on a Rigaku D/MAX 2400 diffractometer equipped with a Cu K_α X-ray source operating at 40 kV and 100 mA (40 kV and 50 mA for small-angle X-ray scanning). *In situ* XRD experiments were carried out as follows: The powder sample was first pressed into a self-supporting wafer and then fixed on the sample holder equipped with a temperature-programmed heater. After the room-temperature X-ray scanning, sample was heated to a specific temperature at 5 K/min ramping rate and kept at that temperature for 1 to 4 h. XRD experiments were performed at each temperature or different time intervals of a specific temperature to observe the agglomeration behavior of silver nanoparticles.

In situ TEM experiments were done on a Philips CM200 Transition Electron Microscope. Sample was first dispersed on a copper grid and then fixed in a special holder equipped with the temperature programmed heater. When a proper region was selected, all experiments were *in situ* performed. The temperature of the grid was increased from room temperature to specific temperature (keeping at that temperature for 30−40 min) until 873 K. TEM images were taken regularly at given heating temperatures or different time intervals to observe the agglomeration behavior of silver nanoparticles. In order to avoid any possible destructive effect of the long time irradiation on the particles and mesoporous walls, the electron beam was switched off during heating.

3. Results and Discussion

3.1. Controlled Fabrication of Monodispersed Silver Nanoparticles within the Channels of SBA-15. In order to produce monodispersed silver nanoparticles, the amino functional groups were grafted to the internal pore walls of SBA-15 using APTS (aminopropyltriethoxyl silane), while silanol groups on the external surface of the silica were terminated/blocked by TMCS (trimethylchlorosilane) treatment. Formaldehyde was then grafted over these amino groups (for details, see Experimental Section). When reacting with adjacent metal precursors such as $Ag(NH_3)_2NO_3$, the *in situ* autoreduction reaction occurred within the mesopores, which enables us to get the monodispersed Ag nanoparticles confined inside the mesopores (Scheme 1).

Figure 1 shows the HRSEM and TEM images of 8 wt % Ag-3/ SBA-15 (Figure 1a,c) and Ag-1/SBA-15 (Figure 1b,d). Silver nanoparticles are present on both the external and internal surface of SBA-15 when the external surface was not treated with TMCS (Figure 1a,c). However, different from that prepared by the traditional incipient impregnation methods (Figure S2), no large silver particles were observed on the external surface of SBA-15 (Figure S3). Instead, they are nearly monodipersed nanoparticles (Figure 1a), indicating that the *in situ* autoreduction route has a good control over the formation of highly dispersed silver nanoparticles, whether they are on the internal or external surface of silica. After deactivation of the silanol groups on the external surface by TMCS, the number of Ag particles on the external surface decreased immediately (Figure 1b), and almost all the monodispersed Ag nanoparticles stayed inside the channels of the mesoporous silica (Figure 1d). This result suggests that by selectively grafting the amino groups, monodispersed silver nanoparticles can be introduced into the mesoporous matrix as we need.

The small-angle XRD pattern of APTS-TMCS-SBA-15 (Figure 2a) indicates that the grafting of amino groups inside the channels did not affect the long-range ordering of the mesostructures. After the loading of Ag into APTS-TMCS-SBA-15, a decrease in intensities of the lower angle peaks was observed (Figure 2b), suggesting that the Ag nanoparticles have been encapsulated inside the pores, which is similar to the case of Pt/SBA-15.[25] The broadening of the Ag diffraction peaks demonstrates that the size of the Ag nanoparticles is in the nanometer range (Inset in Figure 2), which is in good agreement with the TEM observations (Figure 1a).

In the control experiments, if HCHO was not used (Ag-2/SBA-15, i.e., instead a relatively high-temperature treatment was used to get metallic Ag), a mixture of various sized Ag particles and Ag nanowires is observed (Figure 3). If silver ions were first anchored by a complex ($SiCH_2CH_2NH_2$) inside the mesopores, followed by formaldehyde reduction (it is named the

(38) Unger, K. *Angew. Chem., Int. Ed.* **1972**, *11*, 267.

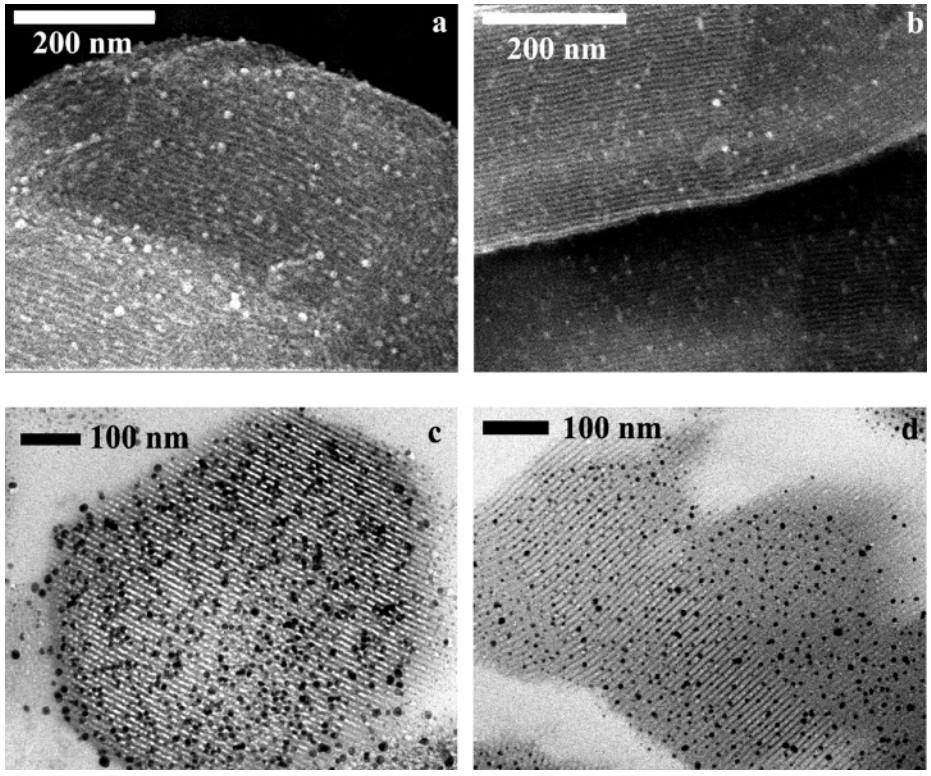

Figure 1. HRSEM (a, b) and TEM images (c, d) of 8 wt % Ag-3/SBA-15 (a, c) and 8 wt % Ag-1/ SBA-15 (b, d).

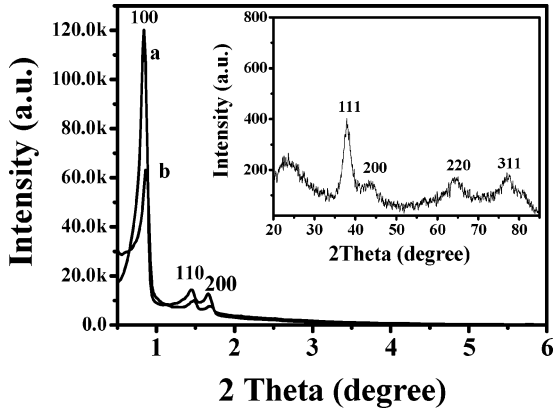

Figure 2. Small-angle XRD patterns of (a) APTS-TMCS-SBA-15; (b) 8 wt % Ag-1/ SBA-15; inset is the wide-angle XRD pattern of 8 wt % Ag-1/SBA-15.

complex-reduction process),[27] silver loading after one cycle of this process is much lower than in that prepared by the *in situ* autoreduction method (Figure S5). At the same time, the multicycle complex-reduction process will lead to diverse distribution of silver nanoparticles in the channels of SBA-15 (Figure S6).

3.2. Fabrication of Highly Dispersed Silver Nanoparticles on Other Silica-Based Materials. It has been proved that the *in situ* autoreduction route is a facile method for the assembly of highly dispersed silver nanoparticles within 2-D mesoporous SBA-15 silica. In fact, it is also suitable to other silica-based materials. Figure 4 shows the typical TEM and HRSEM images of monodispersed silver nanoparticles confined within the channels of various mesoporous silicas (e.g., MCM-41, FDU-12) and on the external surface of silica gels. Indeed, *in situ* autoreduction is an efficient method to synthesize monodispersed silver nanoparticles on silica-based materials (especially, within the channels of the mesoporous silica materials). Significantly, by varying the pore size of mesoporous silicas, it is possible to fabricate monodispersed silver nanoparticles with different particle sizes, which is essential to the investigation of their catalytic properties.

3.3. Formation Mechanism of Highly Dispersed Silver Nanoparticles in the *in Situ* Autoreduction Process. To investigate the formation mechanism of metal nanoparticles within the channels of SBA-15, ^{13}C CP/MAS NMR spectroscopy (Figure 5) was employed to monitor the whole assembly process. Figure 5a shows the ^{13}C CP/MAS NMR spectrum of as-synthesized SBA-15. The signals at 16.3 ppm, 74.5 ppm and its shoulder peak at 70 ppm indicate the existence of the P123 template in the pores.[39] After the functionalization of as-synthesized SBA-15 with TMCS, a new methyl signal at 1.7 ppm appeared (Figure 5b),[40] which suggests that TMCS successfully reacted with external silanol, while the internal silanols remain unaffected due to the protection of occluded templates. The methyl groups on the external surface of SBA-15 are relatively stable upon calcination at 623 K (Figure S7), with a slightly upper field shift which might be related to the slight changes of the circumjacent Si species after the removal of the surfactants. At the same time, the P123 template within the pore channels has been removed completely (Figure 5c), and consequently the exposed internal silanols are accessible to further modification. With APTS treatment, new peaks at 9.5, 16.5, 25.7, 43.9, and 58.3 ppm are observed (Figure 5d). The three stronger signals at 9.5, 25.7, and 43.9 ppm can be ascribed to the resonances of the three methylene groups in the grafted aminopropyl moieties.[41,42] The presence of two weaker peaks at 16.5 and 58.3 ppm indicates that there are some unreacted ethoxy groups left. Combined with the ^{29}Si CP/MAS

(39) Yang, C. M.; Zibrowius, B.; Schmidt, W.; Schüth, F. *Chem. Mater.* **2003**, *15*, 3739.
(40) De, Juan, F.; Ruiz-Hitzky, E. *Adv. Mater.* **2000**, *12*, 430.

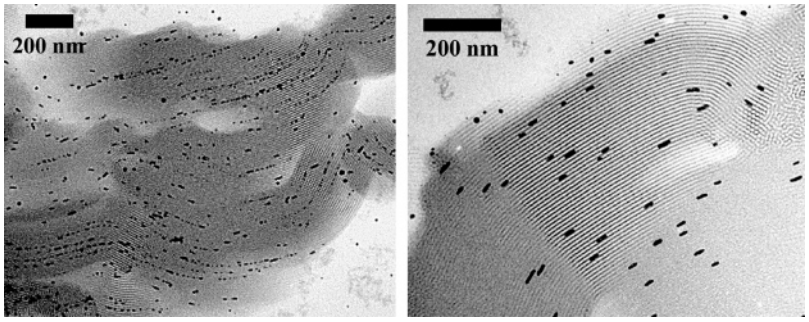

Figure 3. TEM images of Ag-2/SBA-15.

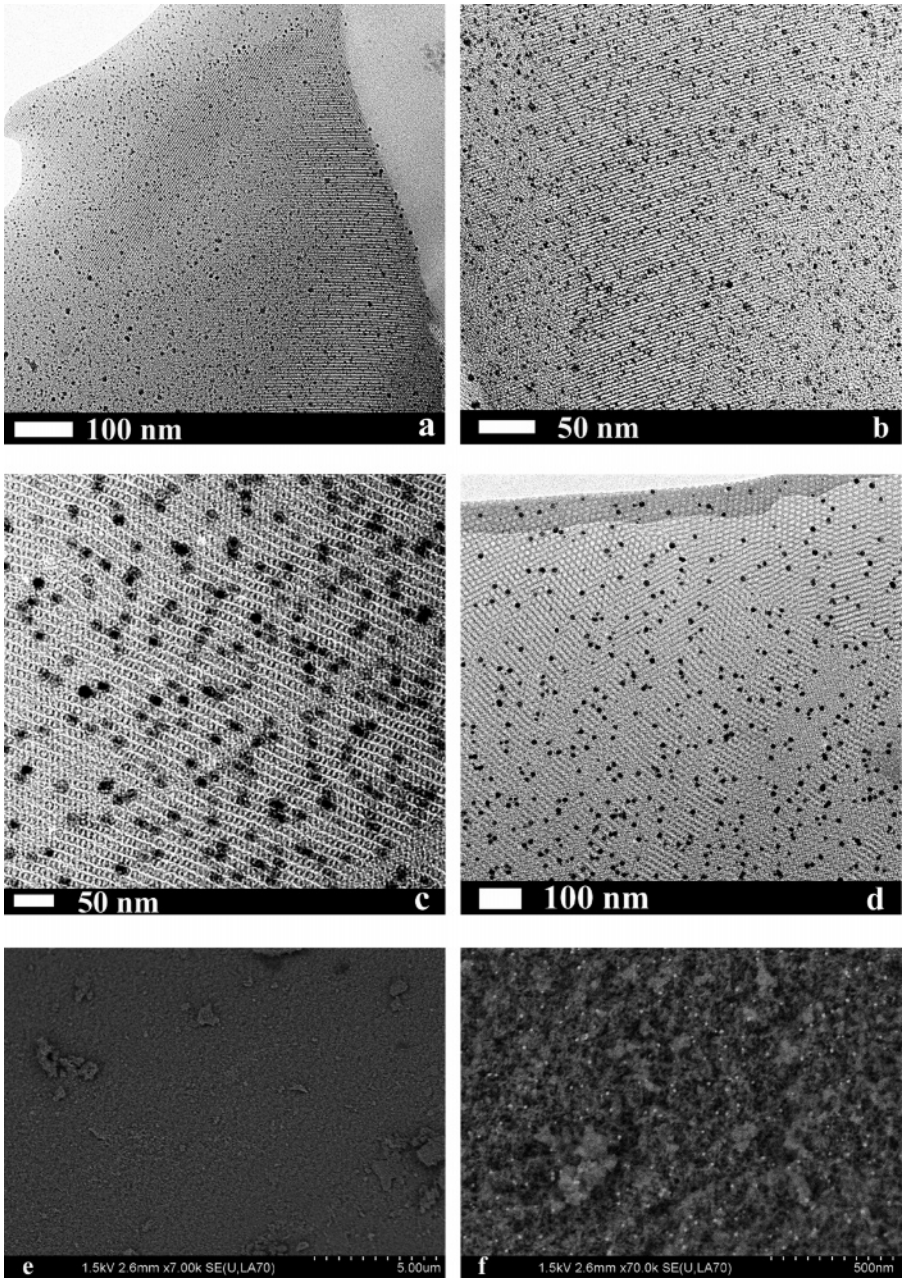

Figure 4. TEM or HRSEM images of (a, b) 8 wt % Ag-1/MCM-41; (c, d) 8 wt % Ag-1/FDU-12 and (e, f) 8 wt % Ag/SiO_2. Bright dots in Figure 4f are silver nanoparticles.

NMR spectrum (Figure S8), it can be concluded that the amino groups have been grafted to the internal pore walls of SBA-15, which is consistent with the nitrogen results (Figure S4 and Table S1).

After the introducion of formaldehyde, another new peak at ca.78.1 ppm appears in the ^{13}C CP/MAS NMR spectrum (Figure 5e). Meanwhile, the signals of C_3 and C_2 shift to lower and higher fields, respectively (Figure 5). This suggests that

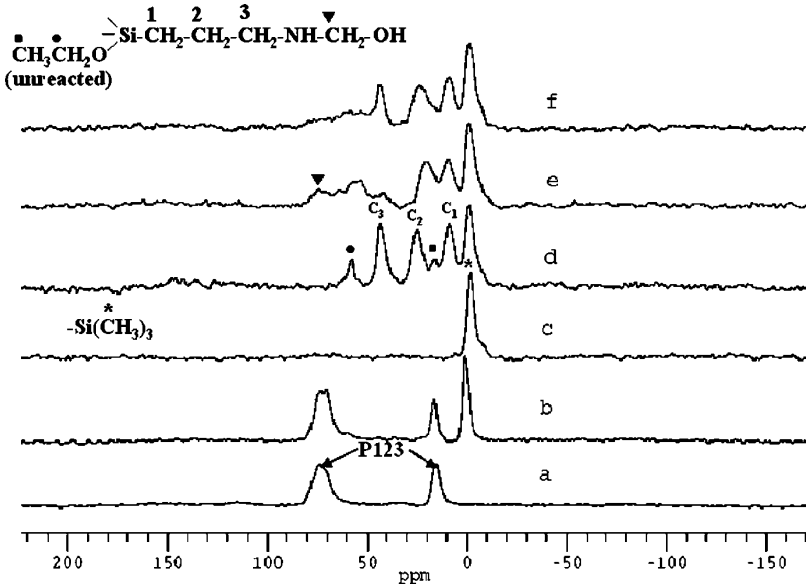

Figure 5. ^{13}C CP/MAS NMR spectra of (a) as-synthesized SBA-15; (b) TMCS-SBA-15 (template included); (c) TMCS-SBA-15; (d) APTS-TMCS-SBA-15; (e) HCHO-APTS-TMCS-SBA-15; (f) Ag-1/SBA-15.

formaldehyde did react with the anchored amino groups on the internal surface of SBA-15, resulting in a new methylene group (78.1 ppm) in $NHCH_2OH$, and the chemical shifts of C_3 and C_2 are also changed due to the alteration of the chemical environment. Interestingly, the signal at 78.1 ppm disappears, and the chemical shifts of the C_3 and C_2 almost revert back to their original positions after the sample reacts with $Ag(NH_3)_2NO_3$ (Figure 5f). This result proves that $NHCH_2OH$ groups are the reductant of silver ions, which makes the assembly of monodispersed Ag nanoparticles practical. The detailed process for the assembly of Ag nanoparticles in the channels of SBA-15 is summarized in Scheme 1.

3.4. Thermal Stabilities of Silver Nanoparticles Confined inside the Channels of SBA-15. 3.4.1.

***In situ* XRD Results.** It should be mentioned that both the fabrication of highly dispersed silver nanoparticles and retention of thermal stabilities are essential to the physical/chemical, especially high-temperature catalytic, properties of these nanoparticles. Herein, *in situ* XRD combined with *in situ* TEM techniques were used to investigate the thermal stabilities of mesoporous silica (e.g., SBA-15)-trapped highly dispersed silver nanoparticles (confined). At the same time, unconfined highly dispersed silver nanoparticles on the external surface of SiO_2 were also studied for comparison.

Figure 6 shows the XRD patterns of confined (i.e., Ag-1/SBA-15, Figure 6a) and unconfined (i.e., Ag/SiO_2, Figure 6b) silver nanoparticles as a function of *in situ* thermal treatment. At room temperature, both samples show broad diffractions that could be indexed to nanosized metallic silver, consistent with the EM observations (Figures 1, 4). Upon thermal treatment in the atmosphere, the intensity and shape of silver diffractions change gradually depending on the temperature and treating time. Obviously, silver nanoparticles confined within the channels of mesoporous SBA-15 and supported over the surface of SiO_2 (unconfined) show different thermal stabilities. Figure 7 illustrates the particle size evaluation during the thermal treatment (calculated by the Scherrer equation).

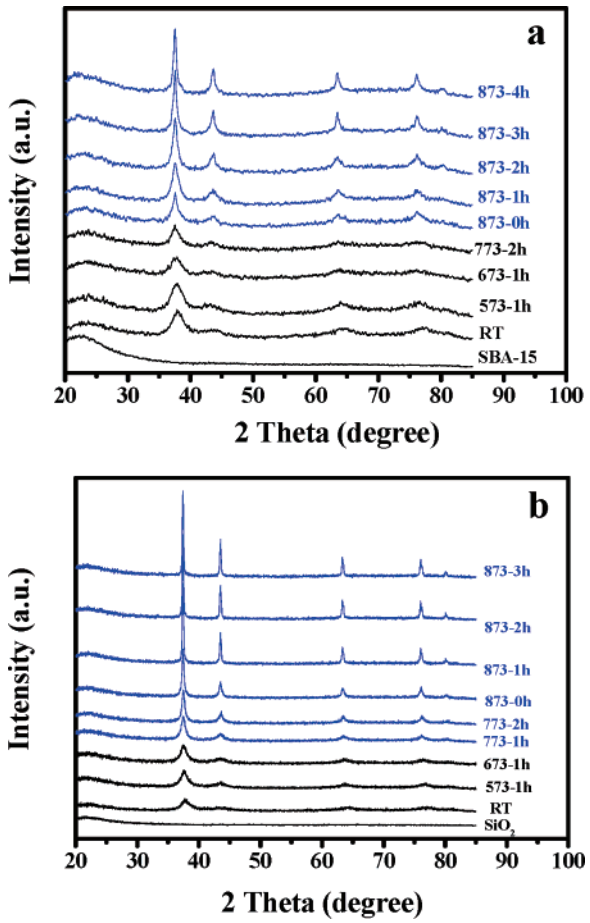

Figure 6. XRD patterns of (a) 8 wt % Ag-1/SBA-15 (confined) and (b) 8 wt % Ag/ SiO_2 (unconfined) as a function of *in situ* thermal treatment at different temperatures and times. RT represents room temperature; 573-1h means that the sample is treated at 573 K for 1 h.

For the SBA-15-confined silver nanopartilcles (Figure 6a), when the temperature is lower than 773 K, no observable change

(41) Liu, M.; Hidajat, K.; Kawi, S.; Zhao, D. *Chem. Commun.* **2000**, 1145.
(42) Huh, S.; Wiench, J. W.; Yoo, J. C.; Pruski, M.; Lin, V. S. Y. *Chem. Mater.* **2003**, *15*, 4247.

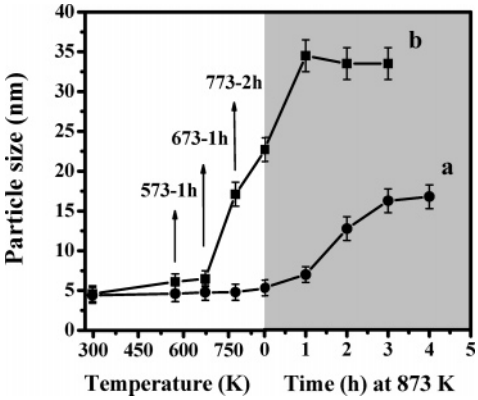

Figure 7. Mean silver particle size evolution toward treating temperature and time (calculated from Figure 6 by the Scherrer equation). (a) 8 wt % Ag-1/SBA-15; (b) 8 wt % Ag/SiO_2.

in its XRD pattern is detected, and the corresponding particle size calculated by the Scherrer equation is the same with that of the as-synthesized sample, i.e., ca. 5 nm. Even if it is treated at 773 K for 2 h, the particle size remains unchanged, suggesting that the silver nanoparticles confined by ordered mesoporous materials can remain stable up to at least 773 K. When the temperature is increased to 873 K, the mean particle size begins to increase slowly, reaching ca. 16 nm when kept at 873 K for 4 h. Compared with the as-synthesized Ag-1/SBA-15 (Figure 1b), substantial amounts of large silver nanoparticles (15−60 nm) are observed on the external surface of SBA-15 (Figure 8a). However, the cross-sectioned TEM images (Figure 8b) show that large amounts of highly dispersed silver nanoparticles are still inside the channels of SBA-15 even after a long-term high-temperature treatment (in this case, 873 K for 4 h). For the unconfined silver nanoparticles, however, another picture (Figure 6b and Figure 7) is presented. The average size of silver nanoparticles increases gradually to ca. 7 nm as the temperature is increased to 673 K. After that (e.g., 773 K), the intensity and sharpness of the diffractions increase very fast, and this trend becomes more obvious at 873 K. The corresponding average particle size evolution diagram (Figure 7b) gives a clear description; i.e., at 773 K, the size of silver nanoparticles increases from ca. 7 nm to ca. 17 nm and then to ca. 34 nm when the temperature reaches 873 K. SEM images of the high-temperature treated Ag/SiO_2 (873 K for 3 h) show that highly dispersed silver nanoparticles have aggregated and larger particles (ca. 15−250 nm) are formed (arrow marked in Figure 8d), and almost no smaller silver particles (below 10 nm) can be observed on the surface of SiO_2 (Figure 8c,d).

3.4.2. *In Situ* TEM Results. From the *in situ* XRD results, it is clear that SBA-15-confined silver nanoparticles show unusual thermal stabilities. To further confirm this point and investigate the underlying aggregation mechanism, *in situ* TEM experiments were employed to study the agglomeration behavior of the SBA-15-confined silver nanoparticles. To compare the different agglomeration behaviors of silver nanoparticles located at the external and internal surface of SBA-15, 8 wt % Ag-3/SBA-15 was selected for the investigation.

To monitor any changes of silver nanoparticles on/in SBA-15 against the thermal treatments, a region is fixed for *in situ* observation. Figure 9a shows a typical TEM image of the Ag-3/SBA-15 at 293 K. Highly dispersed silver nanoparticles located at various positions could be clearly discerned. Nanoparticles located at different chemical/physical positions are selected and marked (Figure 9a). "O" marked the external silver nanoparticles with same chemical environments but different

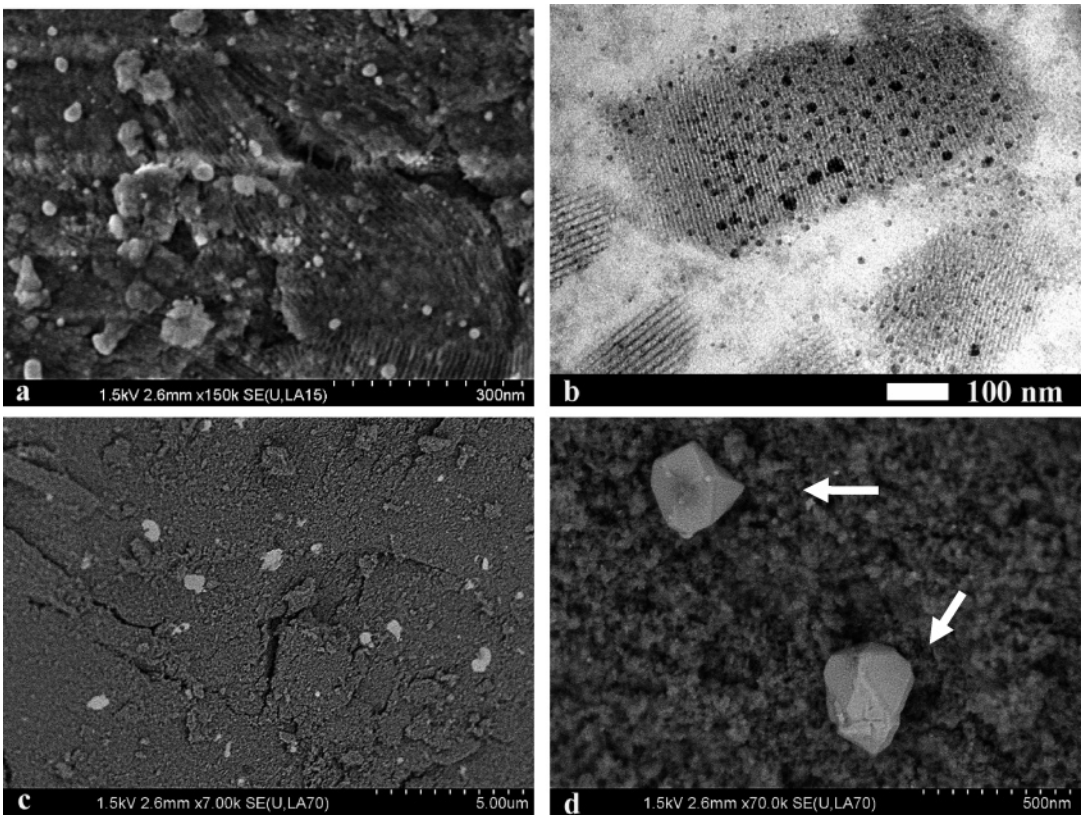

Figure 8. HRSEM or TEM images of (a, b) 8 wt % Ag-1/SBA-15 and (c, d) 8 wt % Ag/SiO_2 after the thermal treating at 873 K for 4 h. Bright dots in the HRSEM images are silver particles.

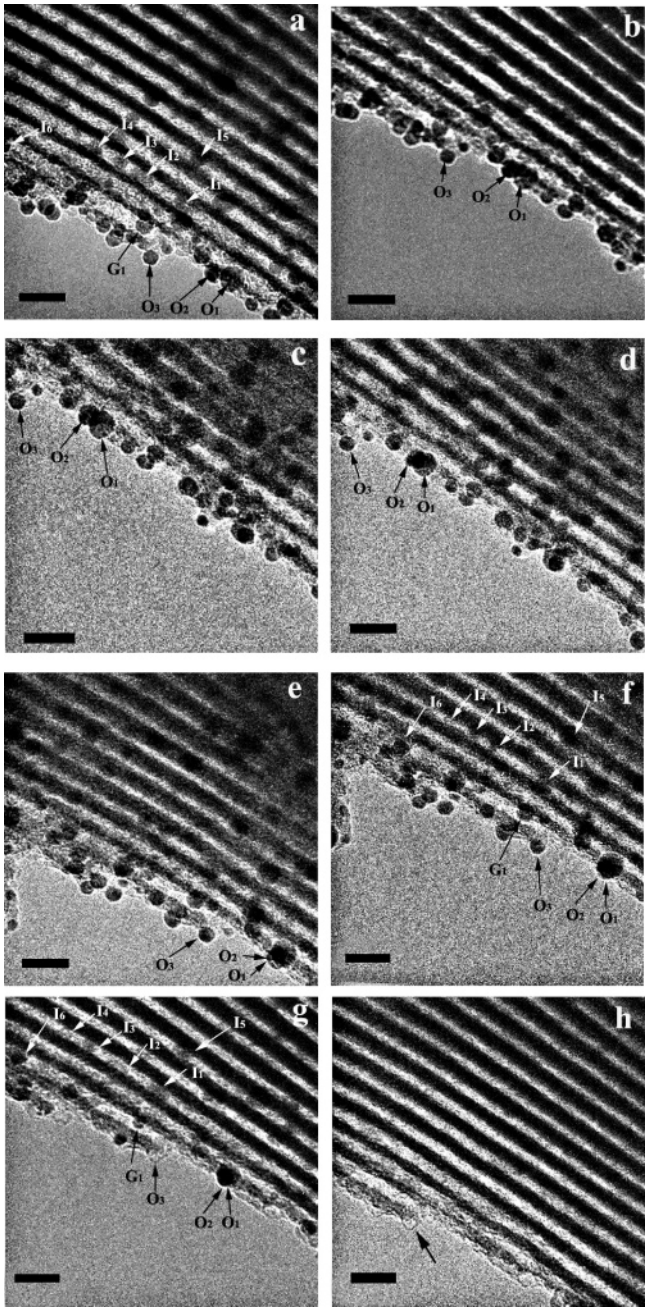

Figure 9. TEM images of 8 wt % Ag-3/SBA-15 annealed at (a) room temperature, (b) 373 K for 30 min, (c) 473 K for 30 min, (d) 573 K for 30 min, (e) 673 K for 30 min, (f) 773 K for 40 min, (g) 873 K for 10 min, and (h) 873 K for 20 min. The scale bars in Figure 9 are all 20 nm.

locations. "I" marked particles trapped inside the mesoporous channels of SBA-15. "G" is one particle located at the orifice, which has the same chemical environment to those "I"-marked particles (confined in mesopores) but should have similar vapor pressure environment to the "O"-marked silver particles.

Figure 9 shows a sequence of TEM images of Ag-3/SBA-15, which is annealed at various temperatures from 293 to 873 K. Clearly, there are two temperature regions, i.e., the low-temperature region (from 293 to 773 K) and the high-temperature region (above 773 K), which is consistent with the *in situ* XRD results.

At the low-temperature region, it was found that the silver nanoparticles show different thermal stabilities, depending on their locations and the treating temperatures. O_1 and O_2 are two closely located silver particles (Figure 9a), the sizes of which are ca. 10 nm, and 6 nm, respectively. They have no obvious changes as time varies at 293 K. On increasing the temperature to 373 K, diffusion and aggregation between O_1 and O_2 are clearly observed (Figure 9b−d). However, the existence of a distinct boundary between particles seems to indicate that the aggregated silver nanoparticles retain their original separated states. Only when the temperature is higher than 673 K, could we observe the fusion of the aggregated silver particles, forming one larger particle, which is ca. 13 nm in size (Figure 9e,f). Significantly, other particles with a relatively larger distance (e.g., O_3) show no obvious coarsening at low temperatures. For silver particles trapped inside the mesoporous channels, however, we could not observe any obvious diffusion and coalescence behavior, though they are closely located (I_1−I_4 in Figure 9a,f), and have been annealed at 773 K for more than 40 min. These results indicate that, compared with the external silver nanoparticles, nanoparticles located inside mesoporous channels are stable even to 773 K, which is in good agreement with the *in situ* XRD results (note that in Figure 6a, Ag-1/SBA-15 was used, which has very limited amounts of silver nanoparticles stayed on the external surface of SBA-15. Thus, the *in situ* XRD results only provide information regarding the SBA-15 confined silver nanoparticles, which is consistent with current *in situ* TEM observation).

At higher temperatures (e.g., 873 K), we still could not observe any diffusion among those internal silver particles; instead, all the silver nanoparticles on SBA-15 disappeared slowly with the treating time, which suggests that the evaporation of silver atoms become predominant at this stage. Interestingly, the disappearance sequence for the silver nanoparticles located at different positions is different. Upon treatment at 873 K for ca. 10 min, silver nanoparticles on the external surface have almost disappeared, while the mesopore-confined silver particles can still be clearly observed (Figure 9g). Significantly, the diameter of the silver nanoparticle located at the orifice decreases from 8 to 6 nm (G1 in Figure 9g). Meanwhile, for the silver nanoparticle with almost the same particles size but a different location (totally inside the channels: I_6 in Figure 9f), no obvious change could be observed. Moreover, the center to center distance between the G_1 and I_6 decreases by ca. 2 nm. Prolonging the treatment for another 10 min (873 K), all the silver nanoparticles trapped inside the silica channels also disappear (Figure 9h). It is interesting to note that some traces are left after the disappearance of silver nanoparticles, which might come from the interfusion between silver and silica substrate during the thermal treatments, indicating the existence of a strong interaction between silver and silica substrate.

It is well-known that the thermal stability of metal nanoparticles is closely related to their Tammann and Hüttig temperatures ($T_{\text{Tammann}} = 0.5T_F$, $T_{\text{Hüttig}} = 0.3T_F$, T_F is the absolute melting temperature). When the treating temperature is higher than the Tammann temperature, atomic mobility increases dramatically. Driven by the tendency to minimize surface energy, metal nanoparticles are apt to agglomerate during the high-temperature treatment, especially when the treating temperature is higher than its Tammann temperature. As a result, interparticle diffusion and subsequent agglomeration/sintering occurred in most cases.[43] Significantly, the melting point of metal nanoparticles decreased drastically with decreasing par-

(43) Moulijn, J. A.; Van, Diepen, A. E.; Kapteijn, F. *Appl. Catal. A* **2001**, *212*, 3.

ticles size.[9] For silver metal, the melting point is only ca. 1233 K, and the $T_{Tammann}$ is ca. 617 K. From this point of view, thermal stability of silver nanoparticles could be much lower, which is confirmed by our *in situ* XRD results of Ag/SiO_2. Surprisingly, *in situ* XRD and *in situ* TEM experiments show that silver nanoparticles confined within the channels of mesoporous SBA-15 silicas could be stable up to 773 K, and this temperature is much higher than Tammann temperature of bulk silver (let along silver nanoparticles). Although *in situ* TEM observation indicates that there are strong interactions between silver and silica substrate, it is not sufficient to stabilize highly dispersed silver nanoparticles at high temperatures, which could be validated by comparing the *in situ* XRD results of Ag/SiO_2 and that of Ag-1/SBA-15, in which both samples employ same kind of substrate (silica), but shows obvious different thermal stabilities of silver nanoparticles. Therefore, the high-thermal stability of silver nanoparticles inside the channels of SBA-15 can only be attributed to the confinement of ordered 1-D mesoporous structures of SBA-15.

Indeed, some unusual physical/chemical properties induced by the confinement of ordered mesoporous silica materials have been reported recently.[44−46] For instance, Dai et al. have prepared nanosized Au catalysts supported over mesoporous silica through a gold cationic complex precursor via a new wet chemical process. They found that Au nanoparticles confined within the mesoporous silica are very stable upon heat treatment.[44] Mou et at. have observed the existence of supercooled water within the 1-D channels of MCM-41.[45] Herein, for silver nanoparticles within the mesoporous channels, no obvious diffusion could be observed by *in situ* TEM during the whole thermal treatment. The reason is still unclear. We propose that the physical confinement of the nanopores and special electronic interactions between silver nanoparticles and mesoporous walls or both contribute to the high-thermal stabilities of the encapsulated silver nanoparticles.

At higher temperatures (e.g., 873 K), *in situ* XRD and *in situ* TEM experiments show obviously different coarsening behavior, which could be attributed to the different conditions of the two systems. Under vacuum conditions, *in situ* TEM shows a sequent disappearance of silver nanoparticles on/in SBA-15, indicating that the evaporation−condensation of silver atoms from silver particles must be predominant at higher temperatures. However, due to the confinement of mesoporous channels, the partial pressure or the concentration of gaseous silver atoms inside the channels would be higher than that of outside space (Scheme 2). Therefore, the evaporation rates of silver atom from the silver particles located on the external surface of SBA-15 would be faster than that of particles located inside the channels. As a result, the external silver particles would disappear first. For the silver particle located at the orifice, due to the difference of concentration and therefore the evaporation rate of gaseous silver atoms between the inner and outer halves of the particles, an anisomerous decay of the particle would result. At the same time, the particle center should move gradually toward the inner pore. Significantly, this mechanism agrees well with the *in situ* TEM observations.

Scheme 2. Schematic Evaporation of Silver Nanoparticles Located at the Orifice and Inner Part of Mesopore Channels[a]

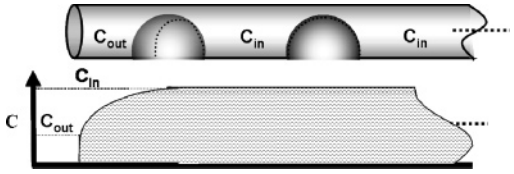

[a] The dot line on the silver particles located at the orifice shows the dimension after the anisomerous decay.

Under atmospheric conditions, *in situ* XRD show a slow but incessant growth of silver particles inside SBA-15 within 4 h at 873 K, suggesting that the coarsening of silver particles is unavoidable even with the confinement of mesopores at temperature as high as 873 K. Combined with the *in situ* TEM results, it can be concluded that the evaporation−condensation of silver atoms (i.e., Ostwald ripening process) would contribute to the coarsening of silver nanoparticles confined inside the channels of SBA-15 at the high temperatures. However, due to the monodipersity of silver nanoparticles and the confinement of mesopores, larger silver particles are mainly created on the external surface of SBA-15.

In situ autoreduction route is a general and facile method for the fabrication of highly dispersed silver nanoparticles over the silica based materials, especially inside the channels of mesoprous silicas. It was demonstrated for the first time by the ^{13}C CP/MAS NMR spectroscopy that amino groups of ATPS-modified MPS can be used to anchor formaldehyde to form $NHCH_2OH$ species, on which $Ag(NH_3)_2NO_3$ could be *in situ* reduced. *In situ* XRD and *in situ* TEM experiments indicate that the confinement of mesopores resulted in an unusual thermal stability of silver nanoparticles trapped inside the channels of SBA-15. It was observed that they could withstand a long-term high temperature (e.g., 773 K, which is much higher than the Tammann temperature of bulk silver (i.e., 617 K)) thermal treatment without any observable coarsening, which is essential to the practical applications in the high-temperature catalytic reactions. On the contrary, silver nanoparticles located on the external surface of SBA-15 or silica gels tended to aggregate via an attractive agglomeration route with the treating temperature close to its Tammann temperature. At higher temperatures (e.g., 873 K), although the coarsening process could be retarded by the confinement of mesoporous channels, silver particles would aggregate through Ostwald ripening inevitably.

Acknowledgment. We are grateful for the support of National Natural Science Foundation of China (No. 90206036) and the Ministry of Science and Technology of China (2005CB221405). J.M. Sun thanks Zhen Zhang (DICP) and Gang Hu (Oxford University) for helpful discussions.

Supporting Information Available: Nitrogen sorption isotherms of SiO_2, Ag/SiO_2, TMCS-SBA-15, APTS-TMCS-SBA-15, and Ag-1/SBA-15; SEM/TEM images of Ag/SBA-15 prepared by the incipient wetness and complex-reduction routes; ^{29}Si NMR spectrum of APTS-TMCS-SBA-15 and TPD-MS spectra of $SBA\text{-}CH_3$. This material is available free of charge via the Internet at http://pubs.acs.org.

JA064884J

(44) Zhu, H. G.; Liang, C. D.; Yan, W. F.; Overbury, S. H.; Dai, S. *J. Phys. Chem. B* **2006**, *110*, 10842.
(45) Liu, L.; Chen, S. H.; Faraone, A.; Yen, C.-W.; Mou, C. Y. *Phys. Rev. Lett.* **2005**, *95*, 117802.
(46) Li, C. *Catal. Rev.* **2004**, *46*, 419.